Transport in Porous Media (2025) 152:112
https://doi.org/10.1007/s11242-025-02246-5

Determination of the Applied Thermal Tortuosity of Porous Media with Macroscopic Geometric Parameters Using a Neural Network Model

Yan Jin[1,2] · **Arne Speerforck**[2] · **Andrey V. Kuznetsov**[3]

Received: 7 January 2025 / Accepted: 21 October 2025

Abstract
The tortuosity of a porous medium has a significant effect on heat transfer through it, but this effect is difficult to quantify. In this study, we have developed the concept of applied thermal tortuosity and the thermal tortuosity function which characterizes the effect of porous medium geometry and the thermal conductivity ratio on the averaged path length of heat conduction in a porous medium. We have also proposed new macroscopic geometric parameters of porous media that can better describe the complexity of the porous media geometry. The relationship between the macroscopic geometric parameters and the developed thermal tortuosity function was established by using a neural network model. We used the developed thermal tortuosity function to calculate effective thermal conductivity, which can be applied in the thermal energy equation. Computations were performed for arbitrary two-dimensional porous media. Despite the model's uncertainties, the developed neural network model is significantly more accurate than empirical correlations for determining the effective thermal conductivity. Optimization of the neural network architecture can further improve the accuracy of the model, but the problem of uncertainty cannot be completely solved. The study shows the importance of embedding the established knowledge of transport in porous media into the neural network model to improve its accuracy.

Keywords Porous medium · Thermal tortuosity · Macroscopic geometric parameters · Neural network model

Abbreviations

CNN	Convolutional Neural Network
FCNN	Fully Connected Neural Network
KINN	Knowledge Informed Neural Network

✉ Yan Jin
yan.jin@tuhh.de

[1] Institute of Multiphase Flows, Hamburg University of Technology, 21073 Hamburg, Germany

[2] Institute of Engineering Thermodynamics, Hamburg University of Technology, 21073 Hamburg, Germany

[3] Department of Mechanical and Aerospace Engineering, North Carolina State University, Raleigh, NC 27695-7910, USA

Published online: 09 November 2025

MSE Mean Squared Error
REV Representative Elementary Volume

Roman Symbols:

A Macroscopic geometric parameters, real part of $\hat{\alpha}$, -
B Macroscopic geometric parameters, imaginary part of $\hat{\alpha}$, -
E Power spectrum of α, -
k_e Effective thermal conductivity, $kg \cdot m \cdot s^{-3} \cdot K^{-1}$
k_f Thermal conductivity in the fluid phase, $kg \cdot m \cdot s^{-3} \cdot K^{-1}$
k_r Reference thermal conductivity, $kg \cdot m \cdot s^{-3} \cdot K^{-1}$
k_s Thermal conductivity in the solid phase, $kg \cdot m \cdot s^{-3} \cdot K^{-1}$
L Straight-line distance, m
L_T Path length of heat conduction throughout a porous network, m
n Scaling coefficient for the effective thermal conductivity correlation, -

Greek Symbols:

α Solid field function, -
α^* Reconstructed solid field function, -
$\hat{\alpha}$ Macroscopic geometric parameters, Fourier coefficients, -
$\alpha^\#$ Pseudo solid field function, -
κ Wave number, m^{-1}
ϕ Porosity, -
λ Heat conductivity ratio, -
Λ_T Applied thermal tortuosity function, -
τ_T Thermal tortuosity, -
τ_T^* Applied thermal tortuosity, -

1 Introduction

A porous medium is a material characterized by a solid matrix and voids (pores). Many materials in nature can be considered porous media, this includes sandstone, wood, soil, human lungs, heat exchangers, etc. (Nield & Bejan 2017). The pore-scale geometry of a porous medium is often highly complex, causing a fluid molecule to travel along a path that is several times longer than the straight line between its original position and its destination. Due to its complexity, the real porous medium geometry is usually not directly simulated when calculating a transport process in a porous medium in engineering applications. Instead, some macroscopic properties of the porous medium are often used to account for the effect of the porous matrix on the transport process, including the porosity (ϕ), permeability (K), mean particle (or fiber) size (d), tortuosity (τ_T), etc. Among these properties, tortuosity is an important parameter, yet its nature is still not fully understood.

Ghanbarian et al. (2012) provide a critical review of the tortuosity models developed empirically, analytically, and numerically for flow in both saturated and unsaturated porous media. They state that, among the commonly applied macroscopic quantities, a clear understanding of tortuosity is still lacking. In practice, tortuosity is not always consistently defined, which can make the concept misleading (Tye 1983; Epstein 1989; Sahimi 1993; Moldrup et al. 2001). The tortuosity is often related to the type of flow or transport process being studied, leading to different definitions of tortuosity between

researchers (Moldrup et al. 2001; Vervoort and Cattle 2003). It remains unclear whether tortuosity is an intrinsic property of the medium, a characteristic of a process within the medium, or simply an ad hoc parameter used to improve the agreement between theory and experiment (Ghanbarian et al. 2012).

The most common definitions of tortuosity include geometric, hydraulic, electrical, and diffusive tortuosity. Geometric tortuosity is defined as the ratio of the average length of the geometric flow through the porous medium to the straight-line distance through the medium (Scheidegger 1974; Adler 1992). Hydraulic tortuosity is defined as the ratio of the flux-weighted average path length for a fluid flow to the straight-line distance (Clennell 1997; Bear 1972). Electrical tortuosity is defined as the ratio of the average path length for an electrical flow to the straight-line distance (Childs 1969; Tindall et al. 1999; Wong 1999). Diffusive tortuosity is defined as the ratio of the average length of a chemical's diffusive pathway to the straight-line distance (Epstein 1989).

It can be observed that each of the above tortuosity definitions corresponds to a specific transport process. However, although heat transfer in porous media is an important transport process, thermal tortuosity—characterizing the path of heat transfer in a porous medium—is not included among the well-established tortuosity definitions reviewed by Ghanbarian et al. (2012). A possible reason for this is that the definition of thermal tortuosity is vague, while it is still not clear whether thermal tortuosity is determined only by the geometry of the porous medium or if it is also related to the thermal properties of the fluid and the solid. The effect of the tortuosity on heat conduction has been considered in some studies (Yang & Nakayama 2010; Yang, et al. 2013; Zhao & Hu 2004). In these studies, well-established tortuosity definitions (such as diffusive tortuosity) are used instead of thermal tortuosity. However, the effect of certain properties related to heat conduction, such as the thermal conductivity ratio, is not accounted for in these tortuosity definitions, hindering the accuracy of the calculations. Thermal tortuosity can be defined as the ratio of bulk thermal conductivity to effective thermal conductivity (Du et al. 2024). However, the bulk thermal conductivity is ambiguously defined and is often regarded as a modeled effective thermal conductivity. Various models exist for its calculation, including the series and parallel models (Winner 1912) and the Maxwell–Eucken model (Callister & Rethwisch 2010). In addition, this approach does not guarantee that the thermal tortuosity will always be greater than or equal to one.

Another difficulty in quantifying the effect of thermal tortuosity is related to the complex geometry of porous media. Tortuosity is conventionally determined by using empirical correlations (Bruggeman 1935; Wyllie & Gregory 1955; Comiti & Renaud 1989; Xu et al. 2018) or through numerical simulations and experiments (Koponen et al. 1996, 1997; Matyka et al. 2008; Du et al. 2024). The correlations are easy to apply, but they may produce significant inaccuracies if the porous medium has a complex geometry. Direct determination of the tortuosity from numerical simulations or experiments is more accurate, but this method is expensive, and the data obtained can only be used in some specific porous medium geometries. In recent years, extensive studies have been carried out to use machine learning methods to predict the macroscopic properties of porous media (Gärttner et al. 2023; Wei et al. 2020; Liu et al. 2022; Yan et al. 2023; Yu et al. 2023; Mesgarpour et al. 2023; Cawte & Bazylak 2022; Huang et al. 2024; Wang et al. 2022). These studies demonstrate the potential of machine learning methods for simulating transport processes in porous media. A key challenge in applying machine learning to predict thermal tortuosity lies in acquiring sufficient training data, which is often costly, and optimizing the neural network's structure.

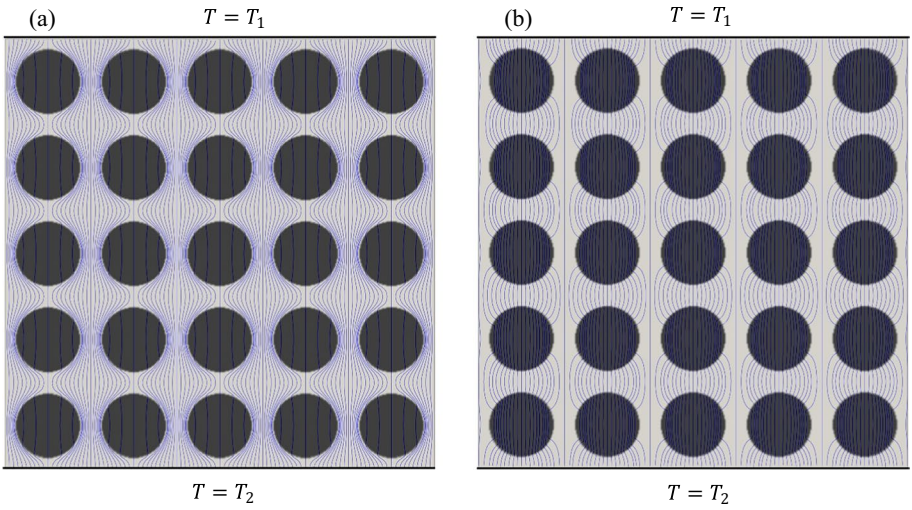

Fig. 1 Path lines of heat conduction (the lines tangential to the temperature gradient) in a porous medium consisting of aligned circular elements. **a** $\lambda = 2 \times 10^{-4}$, **b** $\lambda = 4 \times 10^{3}$

One aim of this study is to propose an easily usable definition of thermal tortuosity that can be quantified by numerical simulations or experiments. In addition, we expect to propose new macroscopic geometric parameters that can represent the complexity of the porous medium geometries. Finally, we will show how thermal tortuosity can be determined with the proposed macroscopic geometric parameters using a neural network model. The paper is structured as follows. In Sect. 2, the basic concepts and mathematical models are introduced. In Sect. 3, using two-dimensional porous media as an example, we demonstrate how a neural network model can be used to determine thermal tortuosity. The effect of the neural network architecture on the accuracy of the model is also analyzed in this section. Finally, Sect. 4 presents the conclusions.

2 Theory and Mathematical Modeling

2.1 Thermal Tortuosity

As explained above, tortuosity is usually defined as the ratio of the average path length for a given process to the straight-line distance. This process may be hydraulic flow, electrical conduction, molecular diffusion, etc. The corresponding tortuosities are called hydraulic, electrical, and diffusive tortuosities, respectively. Similarly, thermal tortuosity is defined as the ratio of the average path length for heat conduction to the straight-line distance in a porous medium with stagnant fluid. Mathematically, thermal tortuosity is expressed as

$$\tau_T = \frac{L_T}{L} \tag{1}$$

where $\langle L_T \rangle$ is the average path length of heat conduction throughout a porous network and L is the straight-line distance.

The definition of thermal tortuosity can be demonstrated using a steady heat conduction problem as shown in Fig. 1. Heat conduction in a porous medium is governed by the following equation

$$\frac{\partial}{\partial x_i}\left(k\frac{\partial T}{\partial x_i}\right) = 0 \tag{2}$$

with a high temperature $T = T_1$ at the top wall and a low temperature $T = T_2$ at the bottom wall. The conductivity of the porous medium is k, which is identical to k_s in the primary (solid) phase and k_f in the secondary (fluid) phase.

The path lines of heat conduction are affected not only by the geometry of the porous medium but also by the heat conductivity ratio $\lambda = \frac{k_s}{k_f}$. Figure 1 illustrates that the porous medium exhibits increased tortuosity for heat conduction as λ deviates from 1. This is different from the hydraulic, electrical, and diffusive tortuosities, which are determined solely by the porous medium geometry.

To solve a heat transfer problem in a porous medium, it is important to know the effective thermal conductivity, which can be used in the macroscopic thermal energy equation. For a porous medium with the thermal conductivity ratio λ, the effective conductivity k_e is calculated as

$$k_e = \frac{Hq_w}{T_1 - T_2} \tag{3}$$

where H is the domain height and q_w is the heat flux at the top (or bottom) wall. Thermal tortuosity τ_T is crucial for the value of k_e, however, it is difficult to determine their relationship mathematically. In addition, it is also difficult to determine τ_T for a porous medium with a complex geometry. Therefore, instead of utilizing the parameter defined by Eq. (1), we introduced a new dimensionless parameter, referred to as the applied thermal tortuosity, which is defined as follows:

$$\tau_T^* = \frac{1}{2}\left(\frac{k_r}{k_e} + \frac{k_e}{k_r}\right) \tag{4}$$

where k_r is a reference thermal conductivity. The applied thermal tortuosity, τ_T^*, characterizes the dimensionless difference between the effective thermal conductivity, k_e, and the reference thermal conductivity, k_r. The parameter τ_T^* reaches its minimum value of 1 when $k_e = k_r$ and increases as k_e diverges from k_r, whether through an increase or decrease. The trend of τ_T^* generally aligns with that of the standard definition of thermal tortuosity τ_T when the thermal conductivity of the primary phase, defined as $\max\left(k_f, k_s\right)$, is used as the reference conductivity in Eq. (4). For a given porous medium geometry, the values of both τ_T and τ_T^* increase as the difference between k_f and k_s increases. For a given k_f and k_s, τ_T^* also becomes larger as the porous medium becomes more tortuous for thermal conduction. As k_s approaches zero, τ_T^* converges to the applied diffusive tortuosity, given by $\frac{1}{2}\left(\frac{D_f}{D_e} + \frac{D_e}{D_f}\right)$, which is a modification of the diffusive tortuosity $\frac{D_f}{D_e}$ as defined in Satterfield

and Sherwood (1963), Greenkorn (1983), and Clennell (1997). Here, D_f and D_e represent the diffusion coefficient in the fluid phase and the effective diffusion coefficient, respectively. The applied diffusive tortuosity also changes monotonically with the diffusive tortuosity. It is important to note that while τ_T^* captures the general trend of τ_T, the two parameters do not take identical values. Their difference is influenced by the geometry of the porous medium.

In this study, the thermal conductivity of the fluid phase k_f is used as the reference thermal conductivity to characterize the difference between k_e and k_f. In addition, we define a tortuosity function Λ_T, the inverse of τ_T^*, as

$$\Lambda_T = \frac{1}{\tau_T^*} = \frac{2}{\frac{k_f}{k_e} + \frac{k_e}{k_f}} \tag{5}$$

Λ_T is bounded between 0 and 1. It is therefore suitable for assessing the accuracy of thermal tortuosity models, as the model error of Λ_T is constrained between -1 and 1. When Λ_T is known and $\Lambda_T \neq 1$, Eq. (5) has two solutions for $\frac{k_e}{k_f}$, one greater than and the other less than one. Thus, the unique value of k_e can be determined from Λ_T according to the value of λ ($\frac{k_e}{k_f} > 1$ if $\lambda > 1$ and $\frac{k_e}{k_f} < 1$ if $\lambda < 1$).

Effective thermal conductivity can also be calculated using empirical correlations. For example, Winner (1912) suggests that k_e can be calculated as

$$k_e = \phi k_f + (1 - \phi) k_s \text{or} \tag{6}$$

$$k_e = \frac{k_f k_s}{\phi k_s + (1 - \phi) k_f} \tag{7}$$

Λ_t can then be determined by substituting Eqs. (6) or (7) into Eqs. (3)-(5).

Alternatively, the dimensionless thermal conductivity ratio can be determined using the following correlation,

$$\frac{\frac{k_e}{k_f} - \lambda}{1 - \lambda} \left(\frac{k_e}{k_f} \right)^{\frac{2}{3}n-1} = \phi \tag{8}$$

see Bruggeman (1935), Solórzanoa et al. (2008), and Yang et al. (2013). However, the coefficient n is related to the geometry of the porous matrix, which must be determined before the correlation is used.

2.2 Macroscopic Geometric Properties

The applied thermal tortuosity is determined by the conductivity ratio λ and the geometry of the porous medium. The porosity ϕ, permeability K, diffusive tortuosity τ_D, mean particle (or fiber) diameter d, etc. are the most commonly used macroscopic properties determined by the porous medium geometry. Obviously, these parameters are not sufficient to describe the complexity of real porous media geometries.

In this study, we propose a new set of macroscopic parameters to characterize the geometry of the porous media by performing a Fourier transform of the solid field function

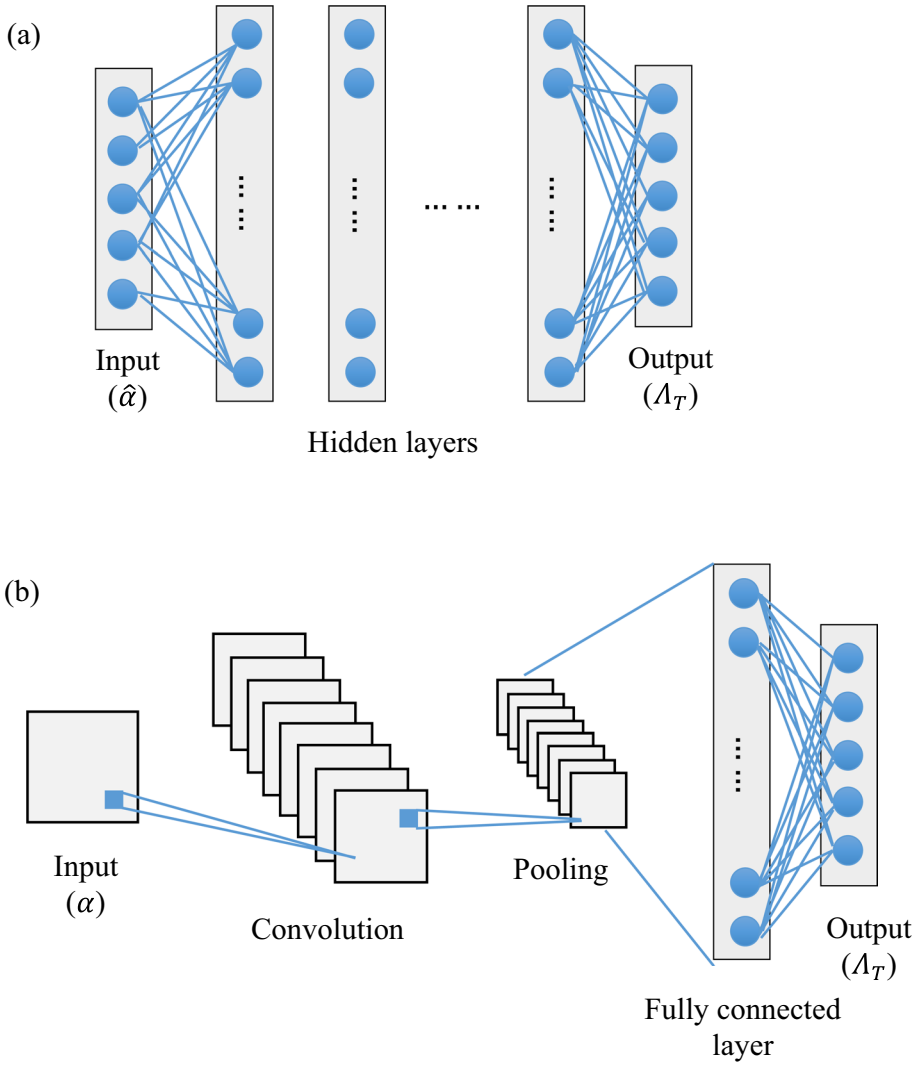

Fig. 2 Diagrams of FCNN (**a**) and CNN (**b**) architectures

α, whose value is 1 in the solid matrix and 0 in the pores. In a three-dimensional representative elementary volume (REV) of a porous medium, we propose using the Fourier coefficients $\hat{\alpha}$ as macroscopic parameters to characterize the geometry of porous media, expressed as

$$\hat{\alpha}(i,j,k) = A(i,j,k) + \bar{i}B(i,j,k) = \left\langle \alpha(x,y,z)\exp\left(-\bar{i}\frac{2\pi}{s}(ix+jy+kz)\right)\right\rangle_{rev} \tag{9}$$

where $\bar{i}$ is the imaginary unit; i,j and k are integers; $A(i,j,k)$ and $B(i,j,k)$ are the real and imaginary parts of the Fourier coefficient $\hat{\alpha}(i,j,k)$; $\langle\,\rangle_{rev}$ denotes the volume averaging in

a REV, which is assumed to be a cubic box; and s is the REV size. Note that $A(0,0,0)$ is the same as the porosity ϕ. Similar to the classical macroscopic properties, $A(i,j,k)$ and $B(i,j,k)$ are all REV-averaged quantities. Using an inverse Fourier transform, the solid field function can be reconstructed as.

$$\alpha^*(x,y,z) = \sum_{i=1-N/2}^{N/2} \sum_{j=1-N/2}^{N/2} \sum_{k=1-N/2}^{N/2} \left(\hat{\alpha}(i,j,k) \exp\left(i \frac{2\pi}{s} (ix + jy + kz) \right) \right) \tag{10}$$

The geometry of the porous medium can be well characterized by the proposed macroscopic parameters when N is large enough. By averaging $\alpha^{*2}(x,y,z)$ in a REV and considering Eq. (9), we can obtain the power spectra of α, expressed as.

$$1 - \phi = \left\langle \alpha^2(x,y,z) \right\rangle_{rev} \approx \left\langle \alpha^{*2}(x,y,z) \right\rangle_{rev} = \sum_{i=1-N/2}^{N/2} \sum_{j=1-N/2}^{N/2} \sum_{k=1-N/2}^{N/2} E\left(\kappa_1, \kappa_2, \kappa_3\right) \tag{11}$$

where the power spectrum $= E\left(\frac{2\pi i}{s}, \frac{2\pi j}{s}, \frac{2\pi k}{s} \right) = A(i,j,k) * A(i,j,k) + B(i,j,k) * B(i,j,k)$. $E\left(\kappa_1, \kappa_2, \kappa_3\right)$ indicates the contribution of the fluctuation of the porous matrix in mode $\left(\frac{2\pi i}{s}, \frac{2\pi j}{s}, \frac{2\pi k}{s} \right)$ to the porosity. Note that $E(0,0,0)$ is identical to $(1-\phi)^2$.

2.3 Machine Learning

Machine learning can establish relationships between the proposed macroscopic geometric properties $\hat{\alpha}$ and the thermal tortuosity function Λ_T for different thermal conductivity ratios. Two types of neural network architectures, the fully connected neural network (FCNN) and the convolutional neural network (CNN), are used in this study. FCNN, also known as a dense neural network, is a type of artificial neural network in which each neuron in one layer is connected to each neuron in the following layer. It consists of an input layer, an output layer, and hidden layers, see Fig. 2a. It is often used as a basic machine learning model but is usually expensive due to the large number of parameters to be trained. CNN is a deep learning neural network that is primarily used for analyzing visual data. A CNN consists of an input layer, an output layer, convolutional layers, pooling layers, and fully connected layers, see Fig. 2b. The CNN is able to handle high-dimensional data efficiently with minimal parameters to train. The FCNN and CNN models are compared in this study when they are used to predict the thermal tortuosity function.

The input data for both FCNN and CNN are the real and imaginary parts of $\hat{\alpha}$, i.e., $A(i,j,k)$ and $B(i,j,k)$ in Eq. (6). The output data are Λ_T at typical thermal conductivity ratios. Two hidden layers were used in an FCNN, while three hidden layers were used in a CNN. The rectified linear unit (ReLU) activation function was used to compute the output neurons of the hidden layers. The open source machine learning library Pytorch 2.5 was used to train the neural networks.

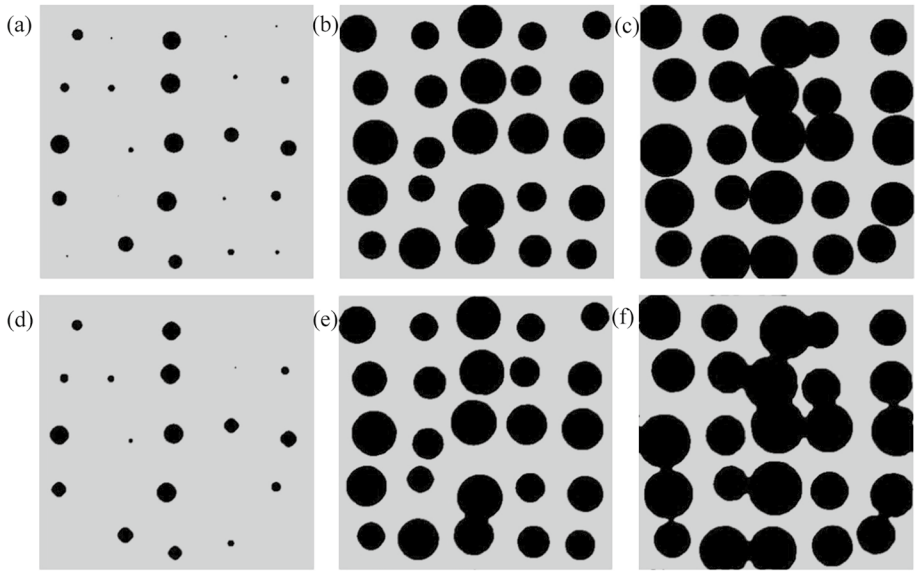

Fig. 3 Original (**a**, **b**, **c**) and reconstructed (**d**, **e**, **f**) porous media consisting of circular porous elements (regular media) with $\phi = 0.96$ (**a**, **d**), $\phi = 0.65$ (**b**, **e**), and $\phi = 0.48$ (**c**, **f**)

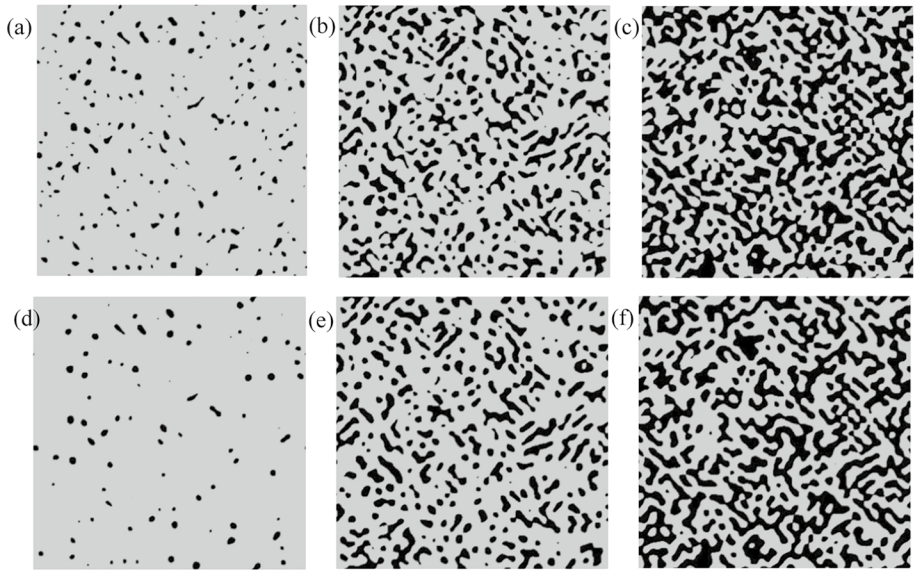

Fig. 4 Original (a, b, c) and reconstructed (**d**, **e**, **f**) porous media consisting of irregular porous elements (irregular media) with $\phi = 0.95$ (**a**, **d**), $\phi = 0.74$ (**b**, **e**), and $\phi = 0.57$ (**c**, **f**)

3 Applications of the Developed Concepts and Methods

The relationship between the thermal tortuosity function Λ_T and the macroscopic

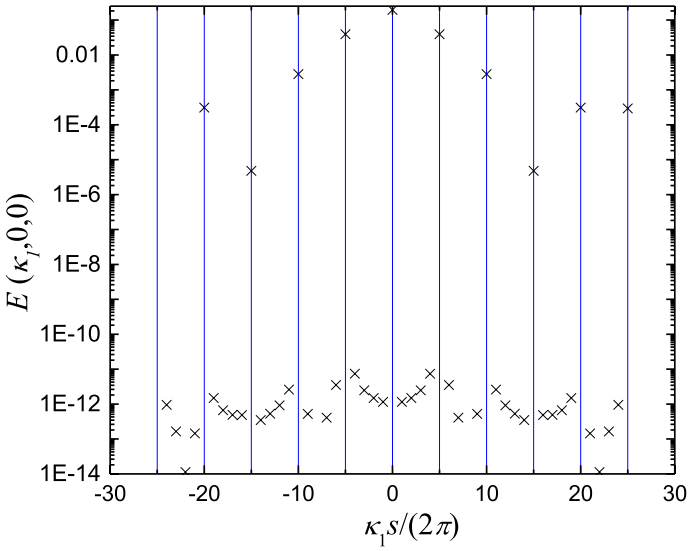

Fig. 5 One-dimensional power spectrum of α in the x-direction, $E(\kappa_1, 0, 0)$, for the porous medium shown in Fig. 1. $E(\kappa_1, 0, 0)$ is close to zero, except when $\kappa_1 s/(2\pi) = 5n$, where n is an integer

geometric parameters $\hat{\alpha}$ is determined for two-dimensional arbitrary porous media to demonstrate the applications of the developed concepts and the machine learning methods. It is assumed that the thermal conductivity is constant, so that the modeled thermal tortuosity function is independent of temperature.

3.1 Generation of Porous Matrices

We generate a series of two-dimensional porous media consisting of circular porous elements (regular media) or irregular elements (irregular media) to obtain training and validation data. The matrices are of the same size, $s \times s$. Similar to the porous matrix shown in

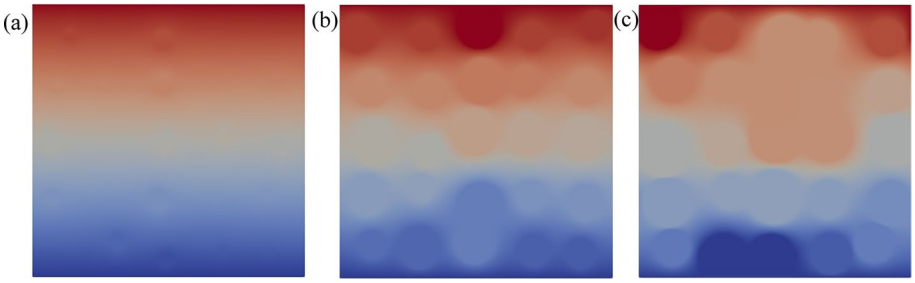

Fig. 6 Temperature fields in the regular media with $\phi = 0.96$ (**a**), $\phi = 0.65$ (**b**) and $\phi = 0.48$ (**c**). $\lambda = 2 \times 10^{-4}$. The corresponding porous media are shown in Fig. 3

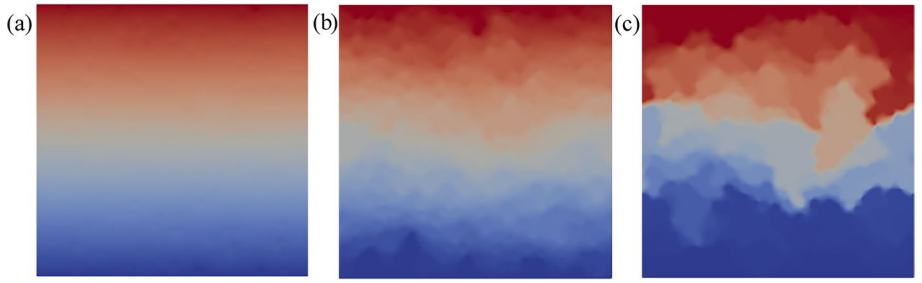

Fig. 7 Temperature fields in the irregular porous media with $\phi = 0.95$ (**a**), $\phi = 0.74$ (**b**), and $\phi = 0.57$ (**c**). $\lambda = 2 \times 10^{-4}$. The corresponding porous media are shown in Fig. 4

Fig. 1, a regular porous matrix consists of 25 (5×5) circular elements, but the circle diameter d and the spacing a have random values. To obtain an irregular porous matrix, we first define a two-dimensional pseudo solid field function

$$\alpha^{\#}(x, y, 0) = \sum_{i=1-N/2}^{N/2} \sum_{j=1-N/2}^{N/2} \hat{\alpha}'(i, j, 0) \exp\left(\frac{2\pi}{s}(ix + jy)\right) \tag{12}$$

where N is set to 50. The real and imaginary parts of the pseudo Fourier coefficients $\hat{\alpha}\prime(i, j, 0)$ have random values varying between 0 and 1. The solid field function is determined as

$$\alpha(x, y, z) = H\left(\alpha^{\#} - \alpha'\right) \tag{13}$$

where H is the Heaviside function which ensures that α is 0 or 1. α' is another random value. The Fourier coefficients $\hat{\alpha}(i, j, 0)$, including their real and imaginary parts $A(i, j, 0)$ and $B(i, j, 0)$, are calculated using Eq. (8). The solid field function can be reconstructed

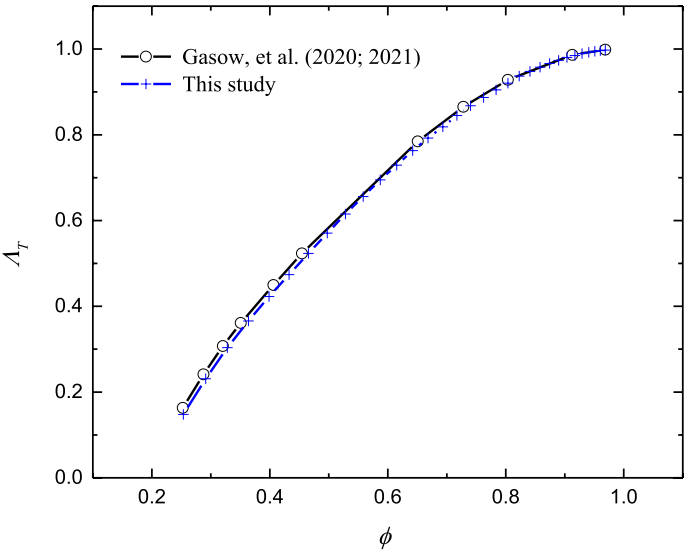

Fig. 8 Comparison of the thermal tortuosity function Λ_T for $\lambda = 2 \times 10^{-4}$ (calculated in this study) and the results for $\lambda = 0$ (Gasow et al. 2020; 2021)

Table 1 Neural networks used to determine the thermal tortuosity function. Two hidden layers are used in FCNNs, and three hidden layers are used in CNNs. The number of neurons in each FCNN layer and the number of channels in each CNN layer are given in the architecture details. The same strides ((4, 2), 2, 2, 4), kernel size (3,3) and padding (0) are used in all CNNs. The optimized neural networks are in gray

ID	Architecture (details)	*nt*	*np*	MSE(i)	MES(r)
FCNN1	FCNN (5000, 1000, 500, 25)	21,712	5,514,025	0.041	0.013
FCNN2	FCNN (5000, 1000, 500, 25)	10,000	5,514,025	0.055	0.014
FCNN3	FCNN (5000, 1000, 500, 25)	5000	5,514,025	0.1	0.019
FCNN4	FCNN (5000, 500, 250, 25)	21,712	2,632,075	0.031	0.012
FCNN5	FCNN (5000, 250, 250, 25)	21,712	1,284,775	0.033	0.012
CNN1	CNN(1, 25, 25, 25, 25)	21,712	17,200	0.052	0.049
CNN2	CNN(1, 50, 50, 50, 25)	21,712	56,875	0.042	0.036
CNN3	CNN(1, 100, 100, 100, 25)	21,712	203,725	0.033	0.027
CNN4	CNN(1, 200, 200, 200, 25)	21,712	767,425	0.031	0.027
CNN5	CNN(1, 300, 300, 300, 25)	21,712	1,691,125	0.043	0.028
CNN6	CNN(1, 100, 200, 100, 25)	21,712	383,825	0.033	0.03

with these macroscopic parameters using Eq. (9). Setting the number of macroscopic geometric parameters N to 50 yields 5000 ($2 \times 50 \times 50$) macroscopic geometric parameters from the Fourier transform (Eq. 8). The original regular and irregular porous matrices are compared to the porous media reconstructed from the macroscopic parameters using Eq. (9) and $\alpha = H(\alpha^* - 0.5)$ in Figs. 3 and 4. The proposed macroscopic parameters effectively capture and describe the characteristics of a porous medium with arbitrary geometry.

The power spectra of the solid field function α can be used to check whether the generated porous matrix is the smallest REV. If a three-dimensional porous matrix of size s consists of smaller periodic structures, the power spectra $E(i, j, k)$ will be dominated by the spectra at fewer wavenumbers $E\left(iN_1, jN_2, kN_3\right)$, where at least one of N_i ($i = 1, 2, 3$) is greater than 1. For the two-dimensional porous matrix shown in Fig. 1, the power spectra are dominated by $E\left(5N_1, 5N_2, 0\right)$, see Fig. 5. Therefore, the smallest REV has the size $(s/5, s/5)$. The porous matrix in Fig. 1 should be reduced to a square with the size $(s/5, s/5)$ before it is used to compute the training and validation data.

3.2 Training and Testing Data

The input data to the neural networks are the 5000 ($2 \times 50 \times 50$) macroscopic geometric parameters for each porous medium. The heat conduction Eq. (1) is solved to determine the heat flux q_w and the effective heat conductivity k_e for the corresponding porous medium at 16 typical heat conductivity ratios: 2^{-12}, 2^{-11},…, 1,… 2^{11}, and 2^{12}. Figures 6 and 7 show the calculated temperature fields in typical regular and irregular media at a low thermal conductivity ratio $\lambda = 2 \times 10^{-4}$ (equal to 2^{-12}). It can be seen that the temperature field varies more strongly as the porosity decreases. The thermal tortuosity functions Λ_T at these 16 typical heat conductivity ratios are used as the output data of the neural network.

To validate the numerical results, the thermal tortuosity function is calculated at a very small thermal conductivity ratio ($\lambda = 2 \times 10^{-4}$) for the porous media consisting of aligned circular elements (see Fig. 1 for the geometry of $\phi = 0.56$). The numerical results are compared with the data from Gasow et al. (2020, 2021), where a body-fitted mesh is used to

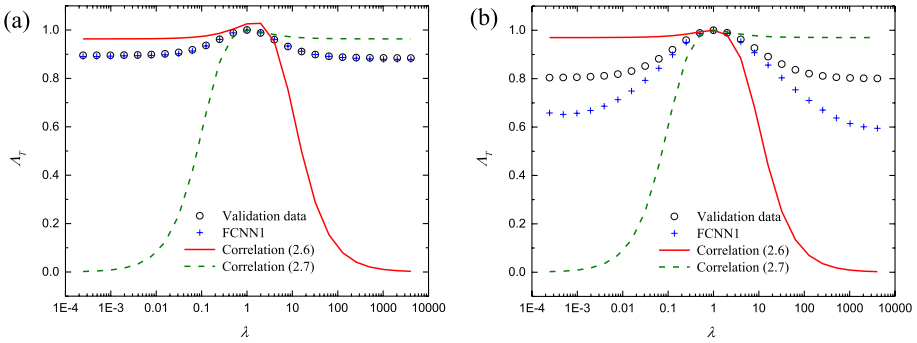

Fig. 9 Comparison of the modeled thermal tortuosity function and the validation data. **a** Regular medium with $\phi = 0.76$, **b** irregular medium with $\phi = 0.81$

determine the diffusive tortuosity (the thermal tortuosity for $\lambda = 0$). Figure 8 shows the good agreement between the two results, validating this study's calculations.

We generated 11,000 regular media and 10,712 irregular media to obtain training data. In each porous medium, 16 calculations were performed to calculate the thermal tortuosity functions at different thermal conductivity ratios. A further 1000 regular and 1000 irregular media were generated to provide validation data to test the neural network model.

3.3 The First Neural Network Model

The original neural network is an FCNN with 1000 and then 500 neurons in the two hidden layers. The neural network is trained using the training data in Sect. 3.2. The mean squared error (MES) loss after the training is 0.013 for the regular porous media and 0.041 for the irregular porous media, see neural network FCNN1 in Table 1. The thermal tortuosity function Λ_T can be determined for any given porous medium using the trained neural network at 16 typical thermal conductivity ratios.

The neural network and correlation results are compared with the validation data in Fig. 9 for two typical porous medium geometries. It can be observed from the validation data that the $\Lambda_t - \ln(\lambda)$ is almost symmetrically distributed. However, this feature is only captured by the neural network model. The correlation Eqs. (6) and (7) cannot identify this feature.

Further model results of Λ_T for different porous media geometries and heat conductivity ratios are compared to the validation data in Figs. 10 (regular media) and 11 (irregular media). The neural network model is significantly more accurate than the correlations but exhibits significant uncertainties at low conductivity ratios. The difference between the model results and the validation data varies between -0.3 and 0.4 at $\lambda = 2 \times 10^{-4}$, as shown in Fig. 11d. In addition, the neural network model exhibits greater uncertainties when applied to irregular media compared to regular media.

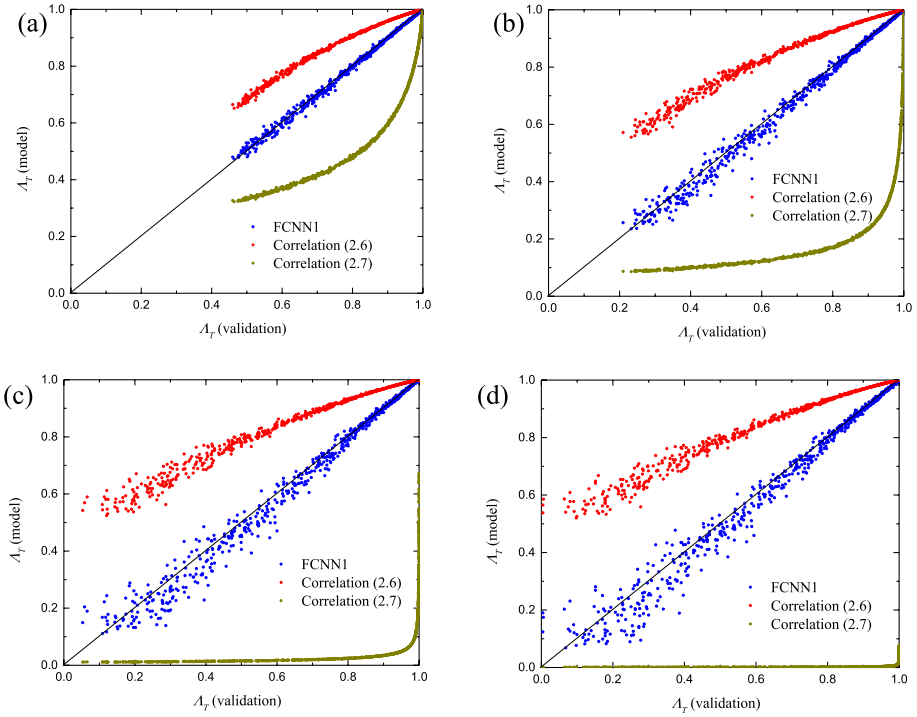

Fig. 10 Modeled the thermal tortuosity function Λ_T versus the validation data for $\lambda = 0.13$ (**a**), 0.03 (**b**), 0.004 (**c**), and 2×10^{-4} (**d**). The model results are compared with the validation data for regular media

3.4 Effect of Neural Network Architecture

The neural network architecture is varied to find an optimized architecture that minimizes the uncertainties of the model results. A possible reason for the uncertainties of the original neural network model (FCNN1) is that it has too many parameters (5,514,025 weights and biases) that need to be trained, but the training data are insufficient due to the high computational cost of obtaining the training data. FCNN1 is trained using 21,712 training data sets. Figure 12 shows the decay of the MSE loss over an epoch during the training process. The results obtained using different numbers of data sets are compared. It can be seen that the MSE loss for training cases becomes lower as the number of data sets is reduced. However, the MSE loss for the testing cases increases with a decrease in the training data due to overfitting.

Besides increasing the training data, which is extremely expensive, the other possible approach to reduce the model uncertainty is to train fewer parameters. Table 1 shows that by reducing the number of neurons in the two hidden layers to 500 and 250 (FCNN3), the MES loss can be reduced to 0.012 for the regular media and 0.031 for the irregular media, respectively. Figures 13 and 14 also show that the model errors are reduced for all thermal conductivity ratios when the neural network architecture is optimized.

Another possible method to reduce the number of parameters is to use CNN architecture. Six CNN architectures are tested in this study. Table 1 shows that model CNN4 has the lowest MES losses (0.027 for regular geometries and 0.031 for irregular geometries)

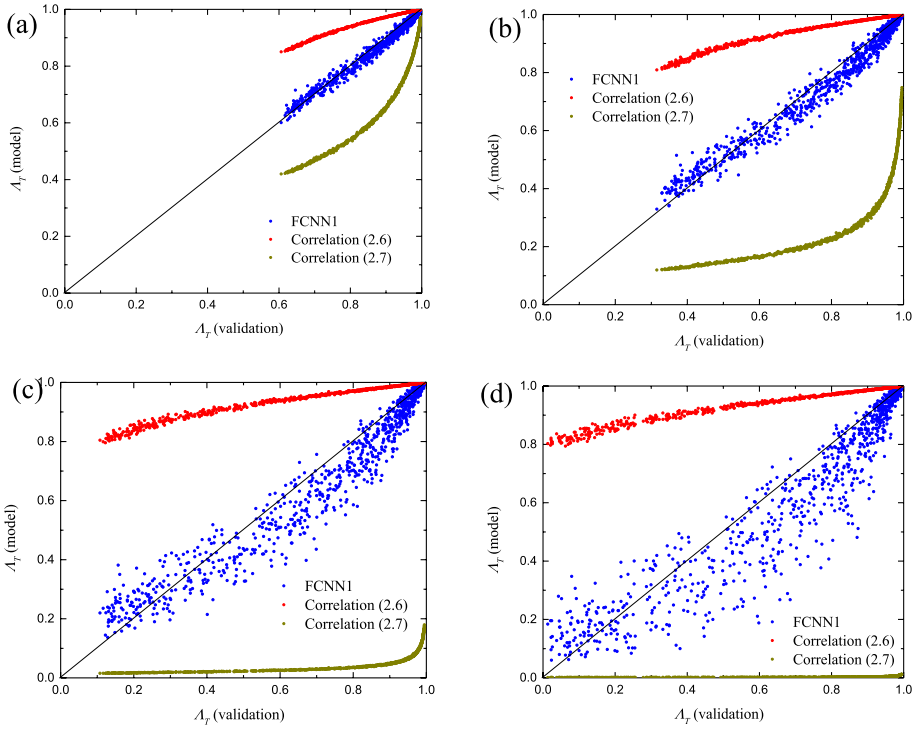

Fig. 11 Modeled thermal tortuosity function Λ_T versus the validation data for $\lambda = 0.13$ (**a**), 0.03 (**b**), 0.004 (**c**), and 2×10^{-4} (**d**). The model results are compared with the validation data for irregular porous media

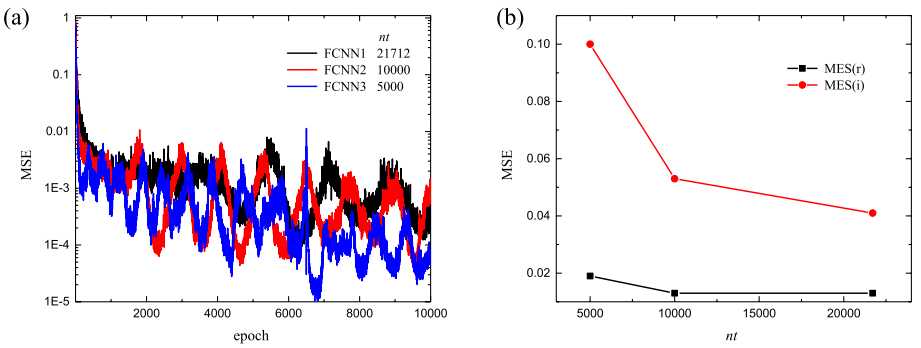

Fig. 12 Decay of the MSE loss over epoch during the training process (**a**) and the MSE loss for the testing data (**b**)

among the CNNs considered. Model CNN4 has a higher accuracy than the other optimized model FCNN3 for irregular porous media with low thermal conductivity ratios ($\lambda \leq 0.004$, see Figs. 14c,d). Due to the symmetry of the $\Lambda_t - \ln(\lambda)$ relationship, model CNN4 also has higher accuracy at very large thermal conductivity ratios ($\lambda \geq 250$). In addition, the accuracy of model CNN4 is only slightly affected by the thermal conductivity ratio and

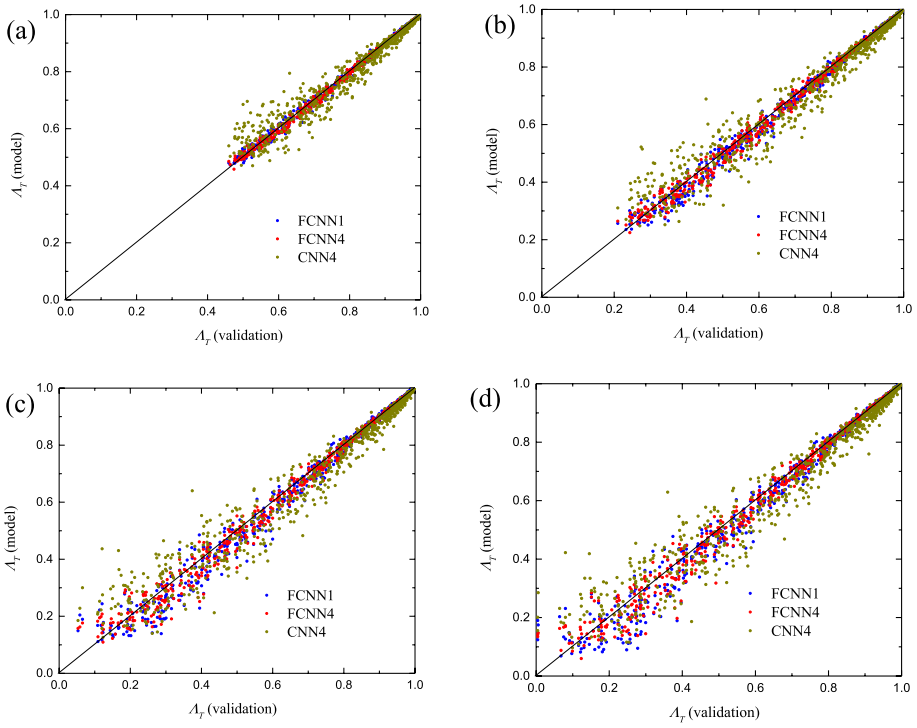

Fig. 13 Modeled thermal tortuosity function Λ_T versus validation data for $\lambda = 0.13$ (**a**), 0.03 (**b**), 0.004 (**c**), and 2×10^{-4} (**d**). The FCNN and CNN results are compared for regular porous media

the geometry of the porous medium. It shows similar accuracy for all cases considered. However, model CNN4 is less accurate than model FCNN3 for regular geometries or when λ is close to 1, see Figs. 13a and 14a. In general, optimizing the architecture of the neural network improves the accuracy of the model but does not completely solve the uncertainty problem.

3.5 Knowledge Informed Neural Network (KINN)

The above discussion shows that sufficient training data is important to ensure the accuracy of a neural network model. However, in practice obtaining sufficient training data is often difficult due to its high cost. A potential solution is to incorporate established knowledge of transport in porous media into the current neural network model. This can reduce the number of parameters that need to be trained.

According to the data-information-knowledge-wisdom (DIKW) hierarchy proposed by Rowley (2007), the knowledge, which is obtained by learning the information, can detect patterns and allow the generation of predictive models. In the training data, it can be observed that the $\Lambda_T - \ln(\lambda)$ profiles are almost symmetric (see Fig. 10), while $\frac{d\Lambda_T}{d\ln(\lambda)} = 0$ when $\lambda = 1$ and $\frac{d\Lambda_T}{d\ln(\lambda)} \to 0$ as $\lambda \to 0$ or $\lambda \to \infty$. Based on these observations, we assumed that the correlation equation for Λ_T has the form.

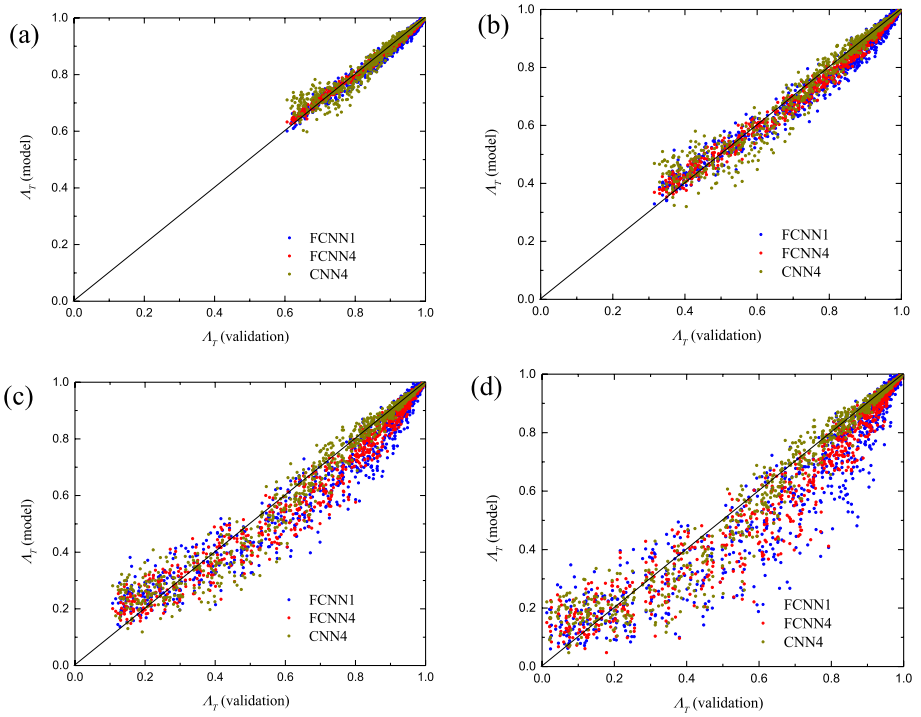

Fig. 14 Modeled thermal tortuosity function Λ_T versus validation data for $\lambda = 0.13$ (**a**), 0.03 (**b**), 0.004 (**c**), and 2×10^{-4} (**d**). The FCNN and CNN results are compared for irregular porous media

$$\Lambda_T = \frac{\lambda^n}{1 + \lambda^{2n}}(1 - A) + A \tag{14}$$

where n and A are the model coefficients.

We introduce a knowledge-informed neural network (KINN) model, depicted in Fig. 15, which is based on Eq. (14). In this KINN architecture, an FCNN is constructed to interrelate the macroscopic geometric parameters (input data) and the model coefficients n and A. Parameters n and A have the same dimension as the output data so that the effect of λ on them is also taken into account. Parameters n and A are substituted into Eq. (14) to determine Λ_T. Each hidden layer uses 100 neurons for the present KINN model. The study in Sect. (3.4) indicates that, with the current number of training data sets, a neural network model with nt in the range $8 \times 10^5 - 2.6 \times 10^6$ has the best performance. The current KINN model uses 1,005,250 neurons, which is within this range.

The KINN results are compared with the FCNN results in Figs. 16 (regular media) and 17 (irregular media). Similar to the CNN model, the KINN model also considerably improves the accuracy for irregular media at low thermal conductivity ratios (Figs. 17c and d). At $\lambda = 2 \times 10^{-4}$, the maximum difference between the model results and the validation data is decreased to 0.2 by the KINN model. In contrast, the maximum difference is 0.4 in the reference FCNN model (FCNN2). In addition, the KINN model is much more accurate for the regular media than the CNN model, see Figs. 13 and 16 for

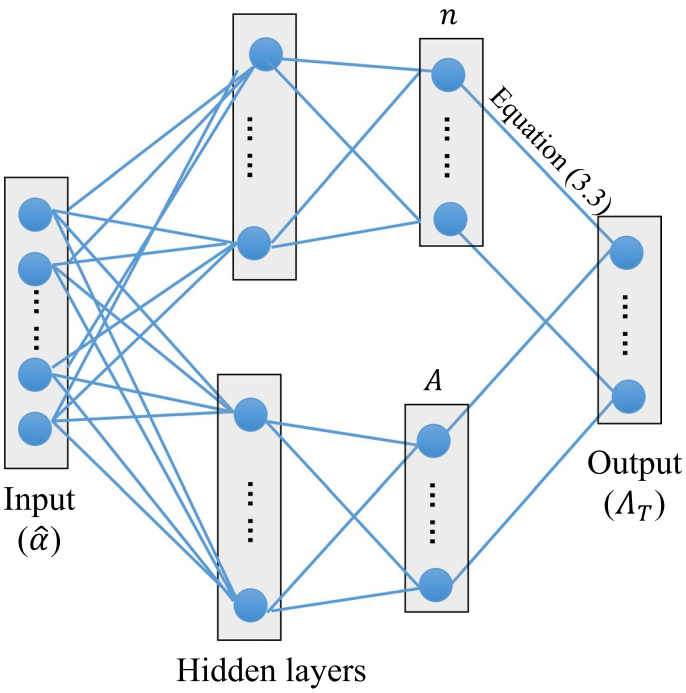

Fig. 15 Diagram of knowledge-informed neural network architecture

comparison. The numerical results show that, with the limited number of neurons (due to the limited number of training data sets), providing established knowledge, such as conservation equations, to the neural network model is a promising method to enhance model accuracy.

The KINN predictions of the dimensionless effective conductivity k_e/k_f are compared with validation data and correlation (8) in Fig. 18 (with $n = 1.8$ for regular porous media and $n = 3$ for irregular porous media) for $\lambda = 0.004$ and 2×10^{-4}. The KINN model accurately predicts effective conductivity without requiring adjustment of its coefficients. Some uncertainty appears at large ϕ values ($\phi \geq 0.96$). This occurs because, as ϕ approaches zero, porosity dominates over other geometric parameters, yet this information is not conveyed to the neural network model.

4 Conclusions

In this study, we have further developed the theory of thermal tortuosity in porous media. The proposed concepts of applied thermal tortuosity τ_T^* and thermal tortuosity function $\Lambda_T = \frac{1}{\tau_T^*}$ effectively characterize the effect of porous medium geometry and thermal conductivity ratio on the average path length of heat conduction in a porous medium. We have also developed new macroscopic geometric parameters of porous media $\hat{\alpha}$ by using a Fourier transform. The proposed parameters effectively capture the complexity of porous

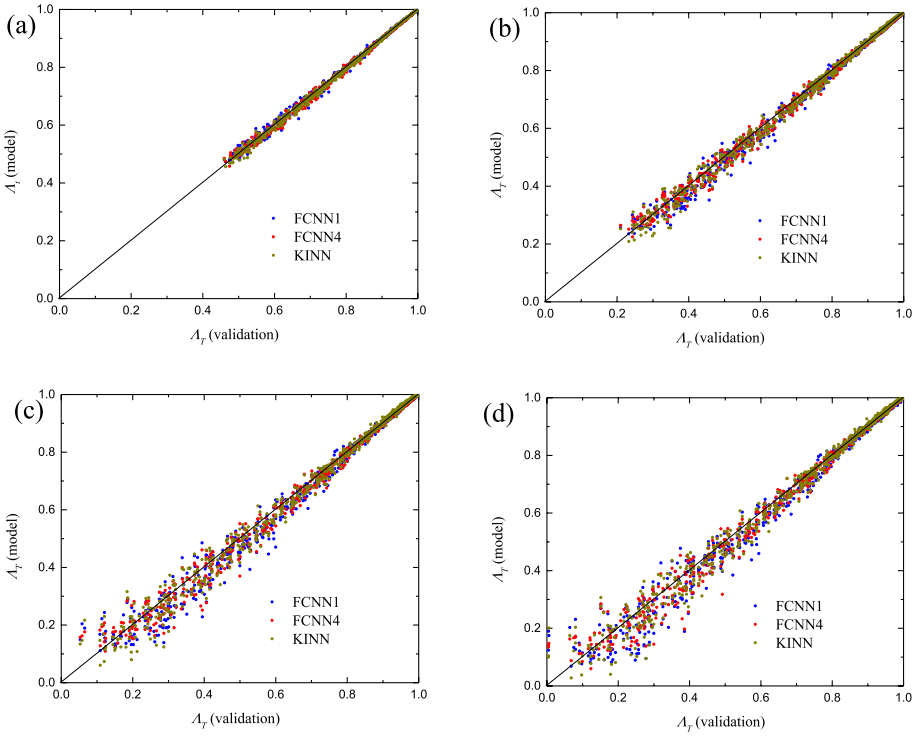

Fig. 16 Modeled thermal tortuosity function Λ_T versus validation data for $\lambda = 0.13$ (**a**), 0.03 (**b**), 0.004 (**c**), and 2×10^{-4} (**d**). The FCNN and KINN results are compared for regular porous media

media geometry. The relationship between the macroscopic geometric parameters $\hat{\alpha}$ and the thermal tortuosity function Λ_T can be established by using a neural network model. The parameter Λ_T of any given porous medium can be accurately determined when the neural network model is fully trained. Substituting the calculated Λ_T into its definition given by Eq. (5), we can determine the thermal conductivity ratio $\frac{k_f}{k_e}$ and, consequently, calculate the effective thermal conductivity k_e. The accurate calculation of k_e is an important step toward an accurate solution of the macroscopic thermal energy equation in porous media. Alternatively, a neural network model could be developed directly to predict the effective thermal conductivity k_e. However, unlike k_e, which is dimensional and ranges from 0 to infinity, Λ_T is a dimensionless parameter bounded between 0 and 1. This makes Λ_T more suitable for use in a neural network model.

Using two-dimensional arbitrary porous media as an example, we have demonstrated the application of the developed concepts and the neural network model. Porous matrices consisting of regular (circular) and irregular porous elements were created to obtain training and validation data. It has been shown how the macroscopic geometric parameters can be used to reconstruct the porous medium and determine the smallest REV. The example studied also shows that the developed neural network model is significantly more accurate than the empirical correlations (6) and (7). However, the present neural network model exhibits considerable uncertainties when the thermal conductivities of the two materials

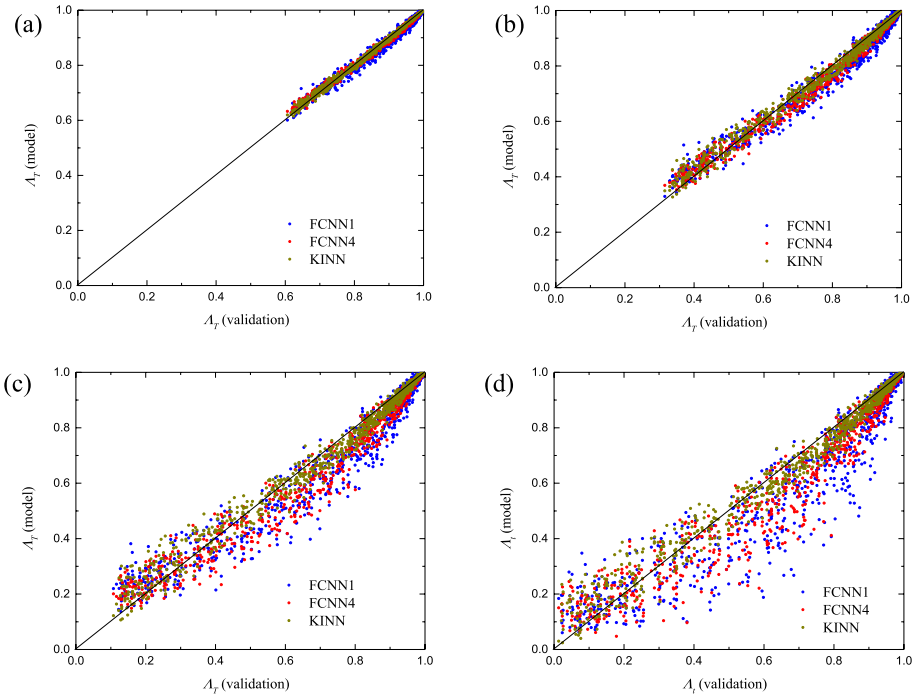

Fig. 17 Modeled thermal tortuosity function Λ_T versus validation data for $\lambda = 0.13$ (**a**), 0.03 (**b**), 0.004 (**c**), and 2×10^{-4} (**d**). The FCNN and KINN results are compared for irregular porous media

within the porous medium are significantly different ($\lambda \ll 1$ or $\lambda \gg 1$). Optimizing the neural network architecture improves the accuracy of the model but does not completely solve the problem of uncertainty. The study shows the importance of embedding established knowledge of transport in porous media into the neural network model and using improved machine learning algorithms, such as CNN, to improve the model accuracy. In addition, the current neural network model is for two-dimensional porous media. It is important to extend the model to three-dimensional porous media, enabling the use of realistic CT-scanned structures to evaluate the model's predictions.

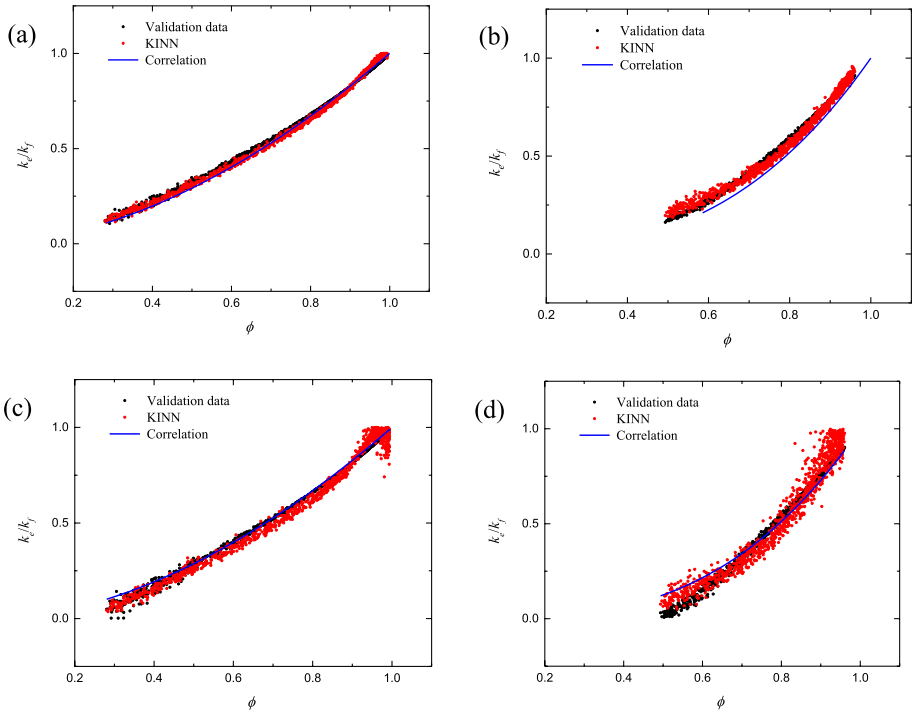

Fig. 18 Comparison of the KINN results for the dimensionless effective conductivity k_e/k_f for regular (**a**, **c**) and irregular porous media (b, d) with the validation data and correlation (8), $\lambda = 0.004$ (**a**, **b**) and $\lambda = 2 \times 10^{-4}$ (**c**, **d**)

Author Contributions All authors contributed to the study conception and design. Material preparation, data collection and analysis were performed by Yan Jin. The first draft of the manuscript was written by Yan Jin and all authors commented on previous versions of the manuscript. All authors read and approved the final manuscript.

Funding Open Access funding enabled and organized by Projekt DEAL. The authors gratefully acknowledge the support of this study by the DFG (Deutsche Forschungsgemeinschaft, 552151258). The computations are performed at the computing center of Hamburg University of Technology (RZ-TUHH). AVK acknowledges the support provided by the National Science Foundation (grant CBET-2042834).

Data Availability The datasets generated and analyzed during the current study are available from the corresponding author upon a reasonable request.

Declarations

Conflict of Interest The authors have no relevant financial or non-financial interests to disclose.

References

Adler, P.M.: Porous media: geometry and transports. Butterworth-Heinemann, Stoneham, MA (1992)
Bear, J.: Dynamics of fluids in porous media. Elsevier, New York (1972)
Bruggeman, D.A.G.: Calculation of various physics constants in heterogenous substances I dielectricity constants and conductivity of mixed bodies from isotropic substances. Ann. Phys. (Berl.). **24**, 636–644 (1935)
Callister, W.D., Rethwisch, D.G.: Materials Science and Engineering: An Introduction. Wiley (2010)
Cawte, T., Bazylak, A.: A 3D convolutional neural network accurately predicts the permeability of gas diffusion layer materials directly from image data. Curr. Opin. Electrochem. **35**, 101101 (2022)
Childs, E.C.: An introduction to the physical basis of soil water phenomena. Wiley-Interscience, New York (1969)
Clennell, M.B.: Tortuosity: A guide through the maze. In: Lovell, M.A., Harvey, P.K. (eds.) Developments in petrophysics, pp. 299–344. Geol. Soc, London (1997)
Comiti, J., Renaud, M.: A new model for determining mean structure parameters of fixed beds from pressure drop measurements: application to beds packed with parallelepipedal particles. Chem. Eng. Sci. **44**, 1539–1545 (1989)
Du, S., Li, D., Li, M.J., He, Y.L.: Numerical study on the effective thermal conductivity and thermal tortuosity of porous media with different morphologies. Sci. China Technol. Sci. **67**, 1685–1694 (2024)
Epstein, N.: On tortuosity and the tortuosity factor in flow and diffusion through porous media. Chem. Eng. Sci. **44**, 777–779 (1989)
Gärttner, S., Frank, F., Woller, F., Meier, A., Ray, N.: Estimating relative diffusion from 3D micro-CT images using CNNs. Artif. Intell. Geosci. **4**, 199–208 (2023)
Gasow, S., Lin, Z., Zhang, H.C., Kuznetsov, A.V., Avila, M., Jin, Y.: Effects of pore-scale on the macroscopic properties of natural convection in porous media. J. Fluid Mech. **891**, A25 (2020)
Gasow, S., Kuznetsov, A.V., Avila, M., Jin, Y.: A macroscopic two-length-scale model for natural convection in porous media driven by a species-concentration gradient. J. Fluid Mech. **926**, A8 (2021)
Ghanbarian, B., Hunt, A.G., Ewing, R.P., Sahimi, M.: Tortuosity in porous media: a critical review. Soil Sci. Soc. Am. J. **77**, 1461–1477 (2012)
Greenkorn, R.A.: Flow phenomena in porous media. Marcel Dekker, NY (1983)
Huang, Q.F., Hong, D.H., Niu, B., Long, D.H., Zhang, Y.Y.: An interpretable deep learning strategy for effective thermal conductivity prediction of porous materials. Int. J. Heat Mass Transf. **221**, 125064 (2024)
Koponen, A., Kataja, M., Timonen, J.: Tortuous flow in porous media. Phys. Rev. E **54**, 406 (1996)
Koponen, A., Kataja, M., Timonen, J.: Permeability and effective porosity of porous media. Phys. Rev. E **56**, 3319 (1997)
Liu, X.C., Park, K., So, M., Ishikawa, S., Terao, T., Shinohara, K., Komori, C., Kimura, N., Inoue, G., Tsuge, Y.: 3D generation and reconstruction of the fuel cell catalyst layer using 2D images based on deep learning. J. Power Sources Adv. **14**, 100084 (2022)
Matyka, M., Khalili, A., Koza, Z.: Tortuosity-porosity relation in porous media flow. Phys. Rev. E **78**, 026306 (2008)
Mesgarpour, M., Habib, R., Shadloo, M.S., Karimi, N.: A combination of large eddy simulation and physics informed machine learning to predict pore-scale flow behaviours in fibrous porous media: a case study of transient flow passing through a surgical mask. Eng. Anal. Bound. Elem. **149**, 52–70 (2023)
Moldrup, P., Olesen, T., Komatsu, T., Schjønning, P., Rolston, D.E.: Tortuosity, diffusivity, and permeability in the soil liquid and gaseous phases. Soil Sci. Soc. Am. J. **65**, 613–623 (2001)
Nield, D.A., Bejan, A.: Convection in Porous media, 5th edn. Springer, Cham, Switzerland (2017)
Rowley, J.: The wisdom hierarchy: representations of the DIKW hierarchy. J. Inform. Sci. **33**(2), 163–180 (2007)
Sahimi, M.: Flow phenomena in rocks: from continuum models to fractals, percolation, cellular automata, and simulated annealing. Rev. Mod. Phys. **65**, 1393–1534 (1993)
Satterfield, C.N., Sherwood, T.K.: The role of diffusion in catalysis. Addison-Wesley, Reading, MA (1963)
Scheidegger, A.E.: The physics of flow through porous media, 3rd edn. Univ. of Toronto Press, Toronto (1974)

Solórzanoa, E., Regleroa, J.A., Rodríguez-Péreza, M.A., Lehmhusb, D., Wichmannb, M., de Saja, J.A.: An experimental study on the thermal conductivity of aluminium foams by using the transient plane source method. Int. J. Heat Mass Transfer **51**, 6259–6267 (2008)

Tindall, J.A., Kunkel, J.R., Anderson, D.E.: Unsaturated zone hydrology for scientists and engineers. Prentice Hall, Englewood Cliffs, NJ (1999)

Tye, F.L.: Tortuosity. J. Power. Sources **9**, 89–100 (1983)

Vervoort, R.W., Cattle, S.R.: Linking hydraulic conductivity and tortuosity parameters to pore space geometry and pore-size distribution. J. Hydrol. **272**, 36–49 (2003)

Wang, M., Wang, H., Yin, Y., Rahardja, S., Qu, Z.G.: Temperature field prediction for various porous media considering variable boundary conditions using deep learning method. Inter. Comm. Heat Mass Trans. **132**, 105916 (2022)

Wei, H., Bao, H., Ruan, X.: Machine learning prediction of thermal transport in porous media with physics-based descriptors. Int. J Heat Mass Trans. **160**, 120176 (2020)

Wong, P.: Conductivity, permeability and electrokinetics. In: Wong, P. (ed.) Methods in the physics of porous media, pp. 115–159. Academic Press, London (1999)

Wyllie, M.R.J., Gregory, A.R.: Fluid flow through unconsolidated porous aggregates. Ind. Eng. Chem. **47**, 1379–1388 (1955)

Xu, W., Jia, M., Gong, Z.: Thermal conductivity and tortuosity of porous composites considering percolation of porous network: from spherical to polyhedral pores. Compos. Sci. Technol. **67**, 134–140 (2018)

Yan, B., Harp, D.R., Chen, B., Pawar, R.: A physics-constrained deep learning model for simulating multiphase flow in 3D heterogeneous porous media. Fuel **313**, 122693 (2023)

Yang, C., Nakayama, A.: A synthesis of tortuosity and dispersion in effective thermal conductivity of porous media. Int. J. Heat Mass Transf. **53**, 3222–3230 (2010)

Yang, X.H., Lu, T.J., Kim, T.: A simplistic model for the tortuosity in two-phase close-celled porous media. J. Phys. D Appl. Phys. **46**, 125305 (2013)

Yu, Y., Chen, S., Wu, Y.H.: Predicting gas diffusion layer flow information in proton exchange membrane fuel cells from cross-sectional data using deep learning methods. Energy **282**, 128778 (2023)

Zhao, A., Hu, Y.: Numerical simulations of effective thermal conductivity in aluminum foam sandwich panel. Therm. Sci. **22**(6B), 2827–2834 (2018)